Cr(III) and Ni(II) Complexes of Isatin-hydrazone Ligand: Preparation, Characterization, Dft Studies, Biological Activity, and Ion-Flotation Separation of Ni(II)

Hany Youssef (hanyyoussef178@gmail.com)
Prince Sattam bin Abdulaziz University https://orcid.org/0000-0001-7671-872X
Yasir Abdulhamed
Prince Sattam bin Abdulaziz University
Tarek Yousef
Imam Mohammad Ibn Saud Islamic University
Gaber Abu El-Reash
Prince Sattam bin Abdulaziz University

Research Article

Keywords: antibacterial study, cytotoxicity, hydrazone derivative, ion-flotation, molecular modeling

Posted Date: July 9th, 2021

DOI: https://doi.org/10.21203/rs.3.rs-682388/v1

Version of Record: A version of this preprint was published at Inorganic Chemistry Communications on February 1st, 2022. See the published version at https://doi.org/10.1016/j.inoche.2022.109278.

Abstract

In the current work, a ligand N'^{1}-((E)-2-hydroxy-3H-indol-3-ylidene)-N'^{3}-((E)-2-oxoindolin-3-ylidene)malonohydrazide (H_4MDI) and its Cr(III) and Ni(II) complexes have been synthesized and characterized by various conventional methods. For evaluating the optimal ligand structure and its complexes, calculations of DFT were applied. Magnetic measurements inherent to their electronic spectra show that both Cr(III) and Ni(II) chelates have octahedron coordination frameworks. On the other hand, the IR spectral data revealed that the ligand behaves as a binegtive hexadentate in $[Cr_2(H_2MDI)(H_2O)_2Cl_4]$ and as a tetranegative hexadentate in $[Ni_2(MDI)(H_2O)_6].4H_2O$. In addition, the behavior of thermal decomposition for prepared complexes was discussed. Two comparable methods (Coats-Redfern and Horowitz-Metzger) were used to calculate the kinetic parameters of the resulted thermal decomposition stages. Furthermore, the ion-flotation process was used for the separation of Ni(II) from aqueous media via the prepared ligand as a chelating agent and oleic acid as a surfactant. Moreover, the antimicrobial behavior of the synthesized moieties was investigated against various bacterial and fungal strains. H_4MDI has the most activity with minimum inhibitory concentration (MIC) of 0.78 µg/mL for both *E. coli,* and *C. Albicans*, while Ni(II) complex shows the activity against *S. aureus, E. coli,* and *C. Albicans* with MIC of 2.34, 4.68, and 1.17 µg/mL, respectively. Finally, the *in-vitro* cytotoxic activity of the prepared compounds against hepatocellular carcinoma human tumor cells (HePG-2) has been examined, and revealed that H_4MDI and its Ni(II) complex show very strong activity against HePG-2 with IC_{50} of 9.7 and 7.7 µmol/L, respectively.

1 Introduction

Today, chemistry and biology are part of our daily world. These two sciences reside at the crossroads of many sectors and industries. Chemists have started to realize that a great number of biochemical molecules are compounds involving one or more metal ions coordinated to groups sometimes large and complex organic. The architectural beauty of these coordination complexes occurs owing to the interesting ligand structures that contain distinct donor locations in heterocyclic rings as well as aliphatic moieties. Schiff bases, also known as azomethines due to they have RC = N group, play important roles in biological systems. They result from condensation reactions between primary amines with carbonyl compounds (aldehydes or ketones) [1, 2]. Schiff base ligands are capable of coordination and stabilization of multiple metal ions in multiple states of oxidation [1, 3]. Because of N–N bond length shortness, the hydrazone ligands mostly act as bi-/tri-or tetradentate moieties although they have the potential to act as bridging tetradentate ligands. Hydrazone ligands also discover countless applications in analytical chemistry, such as transition metal binders. Studies have also shown that the azomethane N with a single pair of electrons in sp^2 hybridized orbital accounts for the biological activity of the hydrazones. The coordination with metal ions also enhances the applications of Schiff Base Ligands. Therefore, in multiple areas, such as luminescent [4–7], catalysis [8, 9], sensors [10–12], and medications [13], this type of compound can be employed. Recently, ion-flotation has received significant attention as a separation technique because of its quickness, easiness, good separation yields, and flexibility of operating and equipment for recovery purposes [14, 15]. In continuation to previous work [16–20] the present work aims to synthesize and characterize Cr(III) and Ni(II) complexes of N'^{1}-((E)-2-hydroxy-3H-indol-3-ylidene)-N'^{3}-((E)-2-oxoindolin-3-ylidene) malonohydrazide (H_4MDI). The modes of chelation and the geometry for the separated complexes are discussed based on DFT calculations and different spectroscopic methods. Moreover, the kinetics and thermodynamic characteristics of the thermal decomposition steps have been studied employing Coats–Redfern and Horowitz–

Metzger models. Also, the application of ion-flotation technique to separate Ni(II) from aqueous solutions was carried out using H_4MDI as chelating agent and oleic acid as a surfactant under the recommended conditions.

2 Experimental

2.1 Materials

All the chemicals used in this study were purchased from Merck Chemical Company, Darmstadt, Germany, and used without any further purification.

2.2 Instrumentation

Elemental analysis (C, H, and N) for the H_4MDI ligand and its complexes were proceeded using a Perkin–Elmer 2400 Series II analyzer, while the content of chloride and metal was done with the referenced procedures [21]. FTIR of H_4MDI and related complexes were recognized on Mattson 5000 FTIR spectrophotometer (4000-400 cm^{-1}). The electronic spectra of the prepared ligand and its complexes mull were done using UV_2 Unicam UV/Vis spectrophotometer using 1-cm stopper quartz cells. The magnetic moment was estimated thru a Sherwood magnetic susceptibility balance. Thermogravimetric analysis (TGA) and differential thermal analysis (DTA) were done on a Shimadzu TGA-50H thermogravimetric analyzer at (20–800^oC) with a nitrogen flow rate of 15 mL/minute and heating rate of 10^oC/minute. The ^{1}H-NMR and ^{13}C-NMR of the prepared ligand were obtained on an Advance DRX 500 Bruker spectrometer (400 MHz) with a 5 mm probe head in d_6-DMSO and chemical shifts are given in parts per million relatives to internal tetramethylsilane (TMS). In the ion-flotation procedure of Ni(II), the concentration of the metal ion was determined using Flame Atomic Absorption Spectrometry (GBC, Sensaa Series) with air-acetylene flame at a wavelength of 232 nm. The flotation cell was a cylindrical tube of 15 mm internal diameter and 290 mm length [22]. The pH of the studied solutions was adjusted using Hanna 8519 digital pH meter.

2.3 Synthesis of ligand

The malonohydrazide was synthesized by the addition of diethyl malonate and hydrazine with a ratio of (1:2) in absolute ethanol placed in an ice bath for 30 min with non-stop stirring, then the resultant substance filtered and washed several times with absolute ethanol and dried in a vacuum desiccator. To prepare the H_4MDI ligand, the prepared material mixed with isatin with a ratio of (1:2) in presence of glacial acetic acid, and the mixture was refluxed on a water bath for a time of (2-4 hours). The products obtained were crystallized several times from absolute ethanol and dried in a vacuum desiccator.

2.4 Synthesis of complexes

Cr(III) and Ni(II) complexes were synthesized via the reflux of H_4MDI ligand with metal salt ($CrCl_3.6H_2O$ or $NiCl_2.6H_2O$) with a ratio of (1:2) in a solution of absolute ethanol placed in a water bath for (2-3 hours). The resulted materials were filtered off, washed several times with ethanol followed by diethyl ether, and finally dried in a vacuum desiccator. H_4MDI ligand and its metal complexes were prepared according to procedures explained in Scheme 1.

2.5 Molecular modeling

DMOL^3 program was applied in the Materials Studio package to estimate the cluster calculations [23]. The optimized configurations of the complexes were predicted by applying the DFT method [24]. DFT calculations and semi-core pseudopods calculations (dspp) were made using the duplicate numerical basis sets plus functional polarization (DNP). The DNP basis was more exact than the Gaussian basis groups of the duplicate extent [25]. The exchange and correlation functional between electrons were described using the revised-Perdew-Burke-Ernzerhof (RPBE) [26] based on the generalized gradient approximation (GGA) functional [27].

2.6 Analytical application (Ion-flotation of nickel)

Suitable aliquots containing a recognized quantity of Ni(II) and H_4MDI ligand were mixed for each investigation. The pH was adjusted to the required value with HNO_3 or NaOH. After that, the solution was moved to the cell of flotation with a total volume of 10 mL adjusted with distilled H_2O and shacked well for 2 minutes to confirm completion of complexation followed by adding 2 mL of surfactant with identified concentration. Then, the cell was shacked well with hand and left 5 minutes standing for confirmation of complete flotation. Finally, the removal % (Re %) of Ni(II) was calculated as follows after its determination by FAAS in the mother liquor:

$$Re\ \% = (M_i - M_f)/\ M_i \times 100 \qquad (1)$$

where: M_i and M_f are referred to the initial and the final concentration of Ni(II), respectively.

2.7 Biological application

2.7.1 Antimicrobial activity

The antimicrobial behavior of the H_4MDI ligand and its corresponding chelates were investigated versus gram-positive bacteria: *Staphylococcus Aureus* (ATCC 12600) and gram-negative bacteria: *Escherichia Coli* (ATCC 11775) as well as *Candida albicans* fungus (ATCC 7102) by an adjusted disc diffusion technique [28]. The solution of each compound such as free ligand, metal complex, and standard drug (Fluconazole “antifungal agent” and Ciprofloxacin “antibacterial agent”) was dissolved in DMSO and prepared for testing versus spore germination.

2.7.2 Antitumor activity

2.7.2.1 Cell line

The studied cell line, Hepatocellular carcinoma (HePG-2), was purchased from VACSERA holding company in Giza, Egypt. Also, 5-fluorouracil was used as a typical anti-cancer medication.

2.7.2.2 MTT assay [29, 30]

The cell line declared above were utilized to investigate the inhibition effects of the isolated ligand and its complexes on cell growth utilizing the MTT inspection [31]. The colorimetric test has been evaluated and recorded by the plate reader (EXL 800, USA) at 570 nm wavelength. The percentage of relative cell viability was calculated as follows:

$$\text{The relative cell viability \%} = \frac{A_{570} \text{ of Treated Samples}}{A_{570} \text{ of Untreated Samples}} \times 100 \quad (2)$$

3 Results And Discussion

Analytical and spectroscopic data for the prepared ligand and its complexes indicate a 1:2 (ligand-metal) stoichiometry for all the complexes. The physical and analytical data of H_4MDI ligand and its metal complexes are given in Table 1. The molecular structures of the metal complexes were confirmed using the data of elemental analyses. All the isolated solid complexes are quite stable in air and insoluble in most of the organic solvents except in dimethylformamide (DMF) and dimethylsulphoxide (DMSO). The thermogravimetric studies of the complexes confirmed high stability which agreed with the high melting points.

3.1 ^{1}H- and ^{13}C-NMR of H_4MDI

The ^{1}H-NMR spectrum (Figure 1) in DMSO exhibited 2 signals at 10.80 and 11.25 ppm which disappeared after the addition of D_2O. These signals are allocated to the protons of $(NH)_{isatin}$ and $(OH)_{enol}$ moieties, respectively. The signal at 2.51 ppm is denoted to the protons of the (CH_2) group. The multi-signals located in the range 6.92-7.54 ppm are referred to as the protons of (CH) of the benzene ring. The strong signal at 8.14 ppm corresponds to the (NH) of the hydrazide side.

The ^{13}C-NMR spectrum (Figure 2) in DMSO displayed 3 signals at 170.18, 165.17, and 102.89 ppm attributed to $(C=O)_{isatin}$., $(C=O)_{hydrazide}$, and $(C=N)_{azomethine}$, respectively.

3.2 IR spectra of H_4MDI and its complexes

A comparison between the IR spectral data of the H_4MDI ligand and its metal complexes was made to study the coordination behavior of H_4MDI toward the studied metal ions. The most important assignments of FTIR absorption bands of H_4MDI and its complexes are displayed in Table 2 and denoted graphically in Figure 1S. FTIR of H_4MDI showed 3 sharp bands at 1733, 1697, and 1611 cm^{-1} assigned to $(C=O)_{isatin}$, $(C=O)_{hydrazide}$, and $(C=N)_{azomethine}$, respectively [16, 17]. The bands located at 3464 (broad), 3237, and 1004 cm^{-1} assigned to (OH) due to enolization, (N-H), and (N-N), respectively. Upon complexation, the (N-N) bands shift to a higher wavenumber [32]. In the binuclear Cr(III) complex, the H_4MDI acts as binegative hexadentate via the $(C=O)_{isatin}$, $(C=N)_{azomethine}$, and the enolized $(C-O)_{hydrazide}$ with deprotonation. This suggestion is confirmed by (i) the appearance of $(C=O)_{isatin}$ at lower wavenumber and disappearance of $(C=O)_{hydrazide}$., (ii) the shift of $(C=N)_{azomethine}$ to higher wavenumber, and (iii) the appearance of new vibration due to (C-O) and the vibration of new (C=N)*. In the binuclear Ni(II) complex, the H_4MDI acts as tetranegative hexadentate via the enolized (C-O) of both hydrazide and isatin moieties with deprotonation and the nitrogen of $(C=N)_{azomethine}$. This mode of chelation is suggested because of (i) the disappearance of vibrations due to both (C=O) (hydrazide and isatin) with the consecutive appearance of new bands due to (C-O) [16] and (C=N), and (ii) the shift of $(C=N)_{azomethine}$ to higher wavenumber.

3.3 Electronic spectra and magnetic properties

The most important assignments of the electronic spectral bands of H_4MDI and its complexes and the values of magnetic moments of the prepared complexes are displayed in Table 3 and denoted graphically in Figure 2S. The spectrum of H_4MDI exhibits an absorption band at 32258 cm^{-1} assigned to ($\pi\rightarrow\pi^*$) of phenyl rings overlapped with that of $(C=N)_{azomethine}$ group. In the region of 22935-27932 cm^{-1}, there is a second intense band that is assigned to ($n\rightarrow\pi^*$) of carbonyl groups that undergo a redshift that suggests the coordination of the oxygen atom of the carbonyl group and the central metal ion [33]. The electronic spectrum of $[Cr_2(H_2MDI)(H_2O)_2Cl_4]$ shows two bands at 22831 and 27932 cm^{-1} assignable to $^4A_{2g}(F)\rightarrow{}^4T_{2g}(F)$ (v_1) and $^4A_{2g}(F)\rightarrow{}^4T_{1g}(F)$ (v_2), respectively, and characterized for an octahedral geometry [34]. The $^4A_{2g}(F)\rightarrow{}^4T_{1g}(P)$ (v_3) band is expected to be at 32051 cm^{-1}. The magnetic moment (3.51 BM) per one metal ion confirms the octahedral structure of $[Cr_2(H_2MDI)(H_2O)_2Cl_4]$. The spectrum of $[Ni_2(MDI)(H_2O)_6].4H_2O$ complex exhibits two absorption bands at 19157 cm^{-1} and 20552 cm^{-1} which be referred to $^3A_{2g}(F)\rightarrow{}^3T_{1g}(F)$ (v_2) and $^3A_{2g}(F)\rightarrow{}^3T_{1g}(P)$ (v_3), respectively [32], which confirm the octahedral structure of $[Ni_2(MDI)(H_2O)_6].4H_2O$. The magnetic moment (2.76 BM) per one metal ion of the complex is also compatible with the suggested geometry.

3.4 Thermal Studies

3.4.1 Thermogravimetric Analysis

Estimation of coordinated or crystallized water molecules can be achieved using TG data [35, 36] (Figure 3S). One can say that there is an agreement between the TG data and the suggested formula. Cr(III) complex has one degradation step in the range (220.53^oC-325.54^oC), indicating the removal of two coordinating water molecules. Ni(II) complex has two degradation steps where the first step in the range (33.09^oC-90.88^oC), indicating the volatilization and removal of four crystalline water molecules with 10.60% weight loss, while the second step in the range (154.10^oC-244.58^oC), corresponding to the removal of six coordinating water molecules. From the thermograms, for the prepared complexes it was concluded that there was a high residual part demonstrating high stability of the prepared complexes. Data for the degradation steps of separated complexes was demonstrated in Table 4.

3.4.2 Kinetic parameters

Coats–Redfern [37] and Horowitz–Metzger [38] methods were used to estimate the thermodynamic and kinetic parameters for the prepared metal complexes as shown in Figures (3-6). Table 5 shows the different parameters (A, E_a, ΔS^*, ΔH^*, and ΔG^*) of the prepared complexes. From the results obtained and listed in Table 5, the following remarks can be pointed out:

1. There is a similarity between the data obtained by the two methods.
2. All decomposition stages followed 1st order (n=1).
3. The high value of the activation energies revealing the high stability of the remaining part of the chelate.

1. The negative ΔS^* values of some degradation stages show that the activated fragments have more ordered structure than the undecomposed one and the degradation reactions are slow [39], while the positive values may suggest that the disorder of the decomposed fragments increases much more rapidly than that of the undecomposed one [40].

2. According to the positive values of ΔH*, the decomposition stages are endothermic.
3. According to the positive values of ΔG*, all the decomposition steps are nonspontaneous.
4. Moreover, the values of ΔG* increase significantly for the subsequent decomposition stages as a result of the increasing of TΔS* which reflects that the rate of removal of the subsequent species is lower than that of the precedent one [41, 42].

According to all previous results, the thermal stability of the metal complexes decreases in the following order: $[Cr_2(H_2MDI)(H_2O)_2Cl_4]$>$[Ni_2(MDI)(H_2O)_6].4H_2O$.

3.5 Molecular Modeling

3.5.1 Geometry optimization

The optimized structures of the ligand and its metal complexes with atomic numbering are given in Figure 7 and recorded in Tables (1S–6S). Upon coordination, the angles of bond for H_4MDI were altered somewhat; the angles that changed upon complexation were O(28)-C(20)-C(19), C(19)-N(18)-N(16), N(18)-N(16)-C(15), O(17)-C(15)-N(16), O(13)-C(12)-N(11), C(12)-N(11)-N(10), N(11)-N(10)-C(9), O(29)-C(8)-C(9). From the review of the measured data for the bond lengths and angles (Tables 1S-6S); supplementary materials, the following can be concluded:

1. After coordination, the bond angles of the ligands were slightly modified, i.e. the bond angles in the ligands were reduced or increased in complex formation as a result of bonding [43].
2. As expected, the formed complexes have bond angles close to an octahedral geometry which predicts hybridization by d^2sp^3 or sp^3d^2 [44].
3. All the active groups that participate in coordination have bonds longer than those already present in the ligand moiety like $(C=O)_{hydrazide}$, $(C=O)_{isatin}$, $(C=N)_{azomethine}$, and $(C=N)_{isatin}$, which refers to resulting from the formation of M–N, and M–O bonds which weakens the (C-N) bond due to coordination via the N atom (C=N) [44].
4. The bond distance of (C=O) extends as the (M-O) bond is formed according to coordination which makes the (C=O) double bond weaker [45].

3.5.2 Global reactivity descriptors

The DFT strategy explains the chemical reactivity and site selectivity of the molecular frameworks. The main parameters in quantum chemical studies are the energies of both HOMO and LUMO. Where HOMO is the highest occupied molecular orbital that acting as an electron donor, and LUMO is the lowest unoccupied molecular orbital that acting as an electron acceptor of electrons. HOMO and LUMO molecular orbitals are recognized as molecular frontier orbitals (FMOs). The energy gap between FMOs describes the stability of the molecule, and this has an important role in calculating electron conductivity, which helps to explain the molecular electrical transport properties. The gaseous phase energies of frontier molecular orbitals (E_{HOMO}, E_{LUMO}), energy bandgap (ΔE) that explains the possible charge transfer interaction within the molecule, electronegativity (χ), global hardness (η), chemical potential (μ), global electrophilicity index (ω), global softness (S) and softness (□) are calculated [46, 47] according to the following equations and listed in Table 6.

$\chi = -1/2\ (E_{LUMO} + E_{HOMO})$	(3)
$\mu = -\chi = 1/2(E_{LUMO} + E_{HOMO})$	(4)
$\eta = 1/2(E_{LUMO} - E_{HOMO})$	(5)
$\Delta E = (E_{HUMO} - E_{LUMO})$	(6)
$S = 1/2\eta$	(7)
$\omega = \mu^2/2\eta$	(8)
$= 1/\eta$	(9)

The outcomes results indicated that:

1. The energy of HOMO and LUMO levels are almost negative showing the stability of the isolated compounds.
2. In the case of ligand, we found that the energy gap is small viewing that charge transfers easily in it and this influences the biological potency, which agrees with experimental data of antibacterial, and antifungal activities. Moreover, the low value of the energy gap is due to the groups that enter into conjugation [48].
3. The low value of energy gap (E_{HOMO}-E_{LUMO}) could be expected to indicate that ligand has a high tendency to coordinate the metal ions, where the molecules with a small gap are known as soft molecules, they are more polarized and reactive than hard molecules as they readily offer electrons to an acceptor.
4. Global hardness and softness are significant properties to measure molecular stability and reactivity. A hard molecule has a large energy gap while the soft one has a small value. During complex formation, the ligand acts as a Lewis base while the metal ion acts as a Lewis acid. Metal ions are soft acids and thus soft base ligands are most effective for complex formation. For that reason, it is concluded that ligand with a proper value of softness has a good tendency to chelate metal ions effectively [49]. This is also confirmed by the calculated chemical potential. The 3D plots for HOMO and LUMO orbital via DFT technique for H_4MDI are illustrated in Figure 8.

3.6 Ion-flotation of Ni(II)

3.6.1 Influence of pH

Several trials were done to test the influence of pH on the removal % of 4×10^{-4} mol/L of Ni(II) using 4×10^{-4} mol/L of H_4MDI and 1×10^{-3} mol/L of HOL. The results were offered in Figure 9. It is clear that maximum removal of Ni(II) (~100%) was attained at the pH (6-9), which facilitates the application of the H_4MDI ligand for the removal of Ni(II) from aqueous media. At pH values higher than 9, the separation efficiency decreased due to the formation of oleates. So, pH 7 was fixed for all subsequent studies.

3.6.2 Influence of nickel concentration

Attempts to remove dissimilar concentrations of Ni(II) with 4×10^{-4} mol/L of H_4MDI and 1×10^{-3} mol/L HOL at pH 7 were done. The results obtained in Figure 10 showed that the optimum removal (~100%) of Ni(II) was attained at the range of (2.5×10^{-4}-4×10^{-4} mol/L) and then decreased sharply and this behavior can be explained as follows:

the prepared ligand gave complete removal of Ni(II) (~100%) which may be due to the presence of enough quantities of ligand to bind all Ni(II) and after 4×10^{-4} mol/L of Ni(II) there is an insufficient ligand. Consequently, 4×10^{-4} mol/L of Ni(II) was used for all subsequent studies.

3.6.3 Influence of H_4MDI concentration

The effect of dissimilar concentrations of prepared ligand on the removal % of 4×10^{-4} mol/L Ni(II) with 1×10^{-3} mol/L HOL at pH 7 was tested. The results were displayed in Figure 11 showed that the removal of Ni(II) increased reaching its optimal removal (~100%) at 4×10^{-4} mol/L of ligand. After that, any excess ligand does not affect the separation process. Consequently, 4×10^{-4} mol/L of H_4MDI was used for all subsequent studies.

3.6.4 Influence of HOL concentration

Experiments were done to remove Ni(II) with HOL only, but the removal does not exceed 36.8 %. So, another run of trials was achieved to remove 4×10^{-4} mol/L Ni(II) in the presence of 4×10^{-4} mol/L of H_4MDI and dissimilar concentrations of HOL (1×10^{-3}-5×10^{-2} mol/L) at pH 7. The results attained and were displayed in Figure 12 showed that in the concentration range of (1×10^{-3}-9×10^{-3}) mol/L of HOL, high removal % of Ni(II) was attained. At a higher concentration of surfactant, the incomplete removal of Ni(II) may be because the high concentration of HOL can change the state of Ni-ligand precipitates which formed through coagulation flotation to re-dispersion form [50]. Furthermore, the decrease in flotation at a higher concentration of HOL is produced by the formation of a stable, hydrated envelope of surfactant on the air bubble surface [51, 52]. Hence, 1×10^{-3} mol/L of HOL was used for all subsequent studies.

3.6.5 Influence of temperature

Trails were performed to remove Ni(II) in a temperature range of (5-80^{o}C) under the optimum parameters. To do this, a solution of Ni(II) and H_4MDI and another one having surfactant were heated or cooled to the same temperature in a water bath. Then, the surfactant was transferred to Ni(II) solution. Then, the mixture was transferred to the flotation cell followed by a removal procedure. The attained results were displayed in Figure 13 showed that removal % (>98%) of Ni(II) in the range 25-65˚C. Thus, 25˚C was used for all subsequent studies.

3.6.6 Influence of interfering ions

Under the ideal parameters estimated for this study, the removal of Ni(II) from aqueous solutions was tested in the presence of large concentrations of several positive and negative ions. The data were presented in Table 7 and indicated that all the studied interfering ions with high concentrations compared to that of Ni(II) do not affect the removal of Ni(II). Consequently, the proposed method can find its applications on water samples with a different matrix.

3.6.7 Application to real water samples

For testing the application of the proposed method, trials were conducted to remove Ni(II) ions added to some real water samples. The removal tests were done using 50 mL clear and filtered solutions at pH 7. The results displayed in Table 8 showed that the removal was acceptable and quantifiable under the optimum parameters of the proposed removal method.

3.7 Biological activity

3.7.1 Antimicrobial evaluation

Ligand and related complexes were tested for their antibacterial activity against *S. aureus* as gram-positive bacteria and *E. coli* as gram-negative bacteria and their antifungal activity against *C. Albicans*. Table 9 provides antibacterial and antifungal MIC (µg/mL) activities. As references for comparing the potency of the tested compounds under the same circumstances, Fluconazole fungicide and Ciprofloxacin bactericide were used. H4MDI has the most potent activity with MIC of 0.78 µg/mL for both *E. coli* and *C. Albicans*. While Ni(II) complex shows the potent activity against *S. aureus* with MIC of 2.34 µg/mL. Ni(II) complex also shows good MIC activity against *E. coli* with 4.68 µg/mL and *C. Albicans* with 1.17 µg/mL, which have the same reference compounds activities. While Cr(III) complex has the lowest activity with MIC of 37.5 µg/mL against *E. coli*, 12.5 µg/mL against *S. aureus,* and 4.68 µg/mL against *C. Albicans*.

3.7.2 Cytotoxicity assay

For such experiments, the values of IC50 were determined in a micromolar unit. The cytotoxicity of 5-Fluorouracil (5-FU) was compared to the cytotoxicity of the free ligand and its complexes. It was noticed that the cytotoxicity was not affected by that chelation with metal. It is important to emphasize that ligand showed almost high to that of Fluorouracil activity (15.10 µmol/L) for HePG-2. These agreeable results encourage us to conduct further experiments in vitro. Moreover, after extra analysis steps, the ligand also exhibited significant activity against the hepatocellular carcinoma human tumor cells screened (HePG-2) cells as a cell growth inhibitor. Therefore, it is essential to further in vitro biological assessment and to study the mechanism of action [53, 54]. From Table 10, H_4MDI and its Ni(II) complex show very strong activity against the hepatocellular carcinoma human tumor cells screened (HePG-2) with IC_{50} of 9.7 and 7.7 (µmol/L).

4 Conclusions

In the current paper, new complexes of Cr(III) and Ni(II) with N'^{1}-((E)-2-hydroxy-3H-indol-3-ylidene)-N'^{3}-((E)-2-oxoindolin-3-ylidene)malonohydrazide (H_4MDI) have been prepared and characterized using different spectroscopic methods. The ligand behaves as bi-negative hexadentate or tetra-negative hexadentate. The proposed structures of both complexes were optimized using DFT calculations. For both complexes, octahedral geometry is indicated in the electronic spectral data and magnetic moment values. The kinetic parameters (E_a, A, ΔH*, ΔS*, and ΔG*) of all thermal degradation steps for the prepared complexes have been estimated by Coats–Redfern and Horowitz–Metzger methods. The ion flotation for H_4MDI as organic chelate for the separation of about 100% of Ni(II) ions procedure is free from interferences, does not affected by rising temperature up to 65˚C (which gives a chance for application to hot wastewater) making the process economic. Moreover, the highest antimicrobial activity was detected in Ni(II) complex. Additionally, H_4MDI and its Ni(II) complex show a very strong cytotoxic activity against HePG-2 (liver carcinoma) with IC_{50} of 9.7 and 7.7 µmol/L, respectively.

Declarations

Funding Not applicable.

Conflict of interest The authors declare that they have no competing interests and non-financial competing interests.

Availability of data and material The data that support the findings of this study are available from the authors upon reasonable request.

Consent to publish All authors approved for publication.

ORCID

Hany M. Youssef http://orcid.org/0000-0001-7671-872X

Gaber M. Abu El-Reash http://orcid.org/0000-0002-0456-7325

References

[1] T. Arun, S. Packianathan, M. Malarvizhi, R. Antony, N. Raman, Bio-relevant complexes of novel N2O2 type heterocyclic ligand: Synthesis, structural elucidation, biological evaluation and docking studies, Journal of Photochemistry and Photobiology B: Biology, 149 (2015) 93-102.

[2] A. Belal, I. El-Deen, N. Farid, R. Zakaria, M.S. Refat, Synthesis, spectroscopic, coordination and biological activities of some transition metal complexes containing ONO tridentate Schiff base ligand, Spectrochimica Acta Part A: Molecular and Biomolecular Spectroscopy, 149 (2015) 771-787.

[3] M. Nath, P.K. Saini, Chemistry and applications of organotin (IV) complexes of Schiff bases, Dalton Transactions, 40 (2011) 7077-7121.

[4] Z. Xu, X. Mao, P. Zhang, H. Li, Y. Wang, M. Liu, L. Jia, Photocatalytic and luminescent properties of three novel complexes based on a pyridine-pyrimidine-hydrazone ligand, Journal of Molecular Structure, 1128 (2017) 665-673.

[5] Y.M. Fadieiev, S.S. Smola, M.Y. Rusakova, E.V. Malinka, N.V. Rusakova, Spectral-luminescent properties of aerosils with adsorbed adducts of Eu (III) tris-β-diketonates and 1, 10-phenanthroline, Journal of Luminescence, 194 (2018) 631-635.

[6] L.-M. Jia, J. Tong, S.-Y. Yu, Neutral coordination polymers of Cobalt (II), Copper (II), Zinc (II) and Manganese (II) β-diketonate complexes with fluorescent anthracene dipyridine: Synthesis, structure and luminescence properties, Journal of Photochemistry and Photobiology A: Chemistry, 355 (2018) 84-93.

[7] J. Huang, L.-H. Huo, Z.-P. Deng, S. Gao, Influence of the [CuI] n (n= 2 and 6) clusters and conformations of flexible bis (pyridyl) ligands on the topological structures and luminescent properties of cuprous iodide complexes, Polyhedron, 122 (2017) 46-54.

[8] P. Servin, R. Laurent, M. Tristany, A. Romerosa, M. Peruzzini, F. Garcia-Maroto, J.-P. Majoral, A.-M. Caminade, Dual properties of water-soluble Ru-PTA complexes of dendrimers: Catalysis and interaction with DNA, Inorganica Chimica Acta, 470 (2018) 106-112.

[9] R. Antony, S.T. David, K. Saravanan, K. Karuppasamy, S. Balakumar, Synthesis, spectrochemical characterisation and catalytic activity of transition metal complexes derived from Schiff base modified chitosan, Spectrochimica Acta Part A: Molecular and Biomolecular Spectroscopy, 103 (2013) 423-430.

[10] L. Tabrizi, H. Chiniforoshan, High-performance room temperature gas sensor based on gold (III) pincer complex with high sensitivity for NH3, Sensors and Actuators B: Chemical, 245 (2017) 815-820.

[11] C.-S. Chu, Y.-L. Lo, Highly sensitive and linear calibration optical fiber oxygen sensor based on Pt (II) complex embedded in sol–gel matrix, Sensors and Actuators B: Chemical, 155 (2011) 53-57.

[12] T.R. Arun, N. Raman, Antimicrobial efficacy of phenanthrenequinone based Schiff base complexes incorporating methionine amino acid: Structural elucidation and in vitro bio assay, Spectrochimica Acta Part A: Molecular and Biomolecular Spectroscopy, 127 (2014) 292-302.

[13] H. Li, C. Xie, R. Lan, S. Zha, C.-F. Chan, W.-Y. Wong, K.-L. Ho, B.D. Chan, Y. Luo, J.-X. Zhang, A Smart Europium–Ruthenium Complex as Anticancer Prodrug: Controllable Drug Release and Real-Time Monitoring under Different Light Excitations, Journal of medicinal chemistry, 60 (2017) 8923-8932.

[14] L. Stoica, M. Dinculescu, C.G. Plapcianu, Mn (II) recovery from aqueous systems by flotation, Water Research, 32 (1998) 3021-3030.

[15] F.M. Doyle, Z. Liu, The effect of triethylenetetraamine (Trien) on the ion flotation of Cu2+ and Ni2+, Journal of colloid and interface science, 258 (2003) 396-403.

[16] T. Yousef, T. Rakha, U. El Ayaan, G.A. El Reash, Synthesis, spectroscopic characterization and thermal behavior of metal complexes formed with (Z)-2-oxo-2-(2-(2-oxoindolin-3-ylidene) hydrazinyl)-N-phenylacetamide (H2OI), Journal of Molecular Structure, 1007 (2012) 146-157.

[17] T. Yousef, G.A. El-Reash, T. Rakha, U. El-Ayaan, First row transition metal complexes of (E)-2-(2-(2-hydroxybenzylidene) hydrazinyl)-2-oxo-N-phenylacetamide complexes, Spectrochimica Acta Part A: Molecular and Biomolecular Spectroscopy, 83 (2011) 271-278.

[18] O.A. El-Gammal, G.A. El-Reash, T. Yousef, M. Mefreh, Synthesis, spectral characterization, computational calculations and biological activity of complexes designed from NNO donor Schiff-base ligand, Spectrochimica Acta Part A: Molecular and Biomolecular Spectroscopy, 146 (2015) 163-176.

[19] T. Yousef, G.A. El-Reash, M. Attia, M. El-Tabai, Comparative ligational, optical band gap and biological studies on Cr (III) and Fe (III) complexes of hydrazones derived from 2-hydrazinyl-2-oxo-N-phenylacetamide with both vanillin and O-vanillin, Chemical Physics Letters, 636 (2015) 180-192.

[20] T. Yousef, G.A. El-Reash, M. El-Tabai, Comparative studies on P-vanillin and O-vanillin of 2-hydrazinyl-2-oxo-N-phenylacetamide and their Mn (II) and Co (II) complexes, Journal of Molecular Structure, 1159 (2018) 246-258.

[21] A.I. Vogel, Vogel'sTextbook of Quantitative Chemical Analysis, 5th ed., Longmans, London, 1991.

[22] S.E. Ghazy, M.A. Kabil, Determination of trace copper in natural waters after selective separation by flotation, Bulletin of the Chemical Society of Japan, 67 (1994) 2098-2102.

[23] B. Delley, Hardness conserving semilocal pseudopotentials, Physical Review B, 66 (2002) 155125.

[24] D. Systèmes, BIOVIA Materials Studio, Dassault Systèmes: San Diego, CA, USA, (2019).

[25] A. Kessi, B. Delley, Density functional crystal vs. cluster models as applied to zeolites, International journal of quantum chemistry, 68 (1998) 135-144.

[26] B. Hammer, L.B. Hansen, J.K. Nørskov, Improved adsorption energetics within density-functional theory using revised Perdew-Burke-Ernzerhof functionals, Physical review B, 59 (1999) 7413.

[27] A. Matveev, M. Staufer, M. Mayer, N. Rösch, Density functional study of small molecules and transition-metal carbonyls using revised PBE functionals, International journal of quantum chemistry, 75 (1999) 863-873.

[28] M.A. Pfaller, L. Burmeister, M. Bartlett, M. Rinaldi, Multicenter evaluation of four methods of yeast inoculum preparation, Journal of clinical microbiology, 26 (1988) 1437-1441.

[29] T. Mosmann, Rapid colorimetric assay for cellular growth and survival: application to proliferation and cytotoxicity assays, Journal of immunological methods, 65 (1983) 55-63.

[30] S.M. Baksi, J.M. Frazier, Isolated fish hepatocytes—model systems for toxicology research, Aquatic Toxicology, 16 (1990) 229-256.

[31] T.L. Riss, R.A. Moravec, A.L. Niles, S. Duellman, H.A. Benink, T.J. Worzella, L. Minor, Cell viability assays, Assay Guidance Manual [Internet], (2016).

[32] T. Yousef, O. Alduaij, S.F. Ahmed, G.A. El-Reash, O. El-Gammal, Semi-and thiosemicarbazide Mn (II) complexes: Characterization, DFT and biological studies, Journal of Molecular Structure, 1119 (2016) 351-364.

[33] R.S. Joseyphus, C.J. Dhanaraj, M.S. Nair, Synthesis and characterization of some Schiff base transition metal complexes derived from vanillin and L (+) alanine, Transition metal chemistry, 31 (2006) 699-702.

[34] T. Yousef, O. Alduaij, S.F. Ahmed, G.A. El-Reash, O. El-Gammal, Structural, DFT and biological studies on Cr (III) complexes of semi and thiosemicarbazide ligands derived from diketo hydrazide, Journal of Molecular Structure, 1125 (2016) 788-799.

[35] T. Rakha, K. Ibrahim, M. Khalifa, Thermochemical study of some transition metal complexes of isonicotinic hydrazide derivatives, Thermochimica acta, 144 (1989) 53-63.

[36] R. Zaky, T. Yousef, A. Abdelghany, Computational studies of the first order kinetic reactions for mononuclear copper (II) complexes having a hard–soft NS donor ligand, Spectrochimica Acta Part A: Molecular and Biomolecular Spectroscopy, 130 (2014) 178-187.

[37] A.W. Coats, J. Redfern, Kinetic parameters from thermogravimetric data, Nature, 201 (1964) 68-69.

[38] H.H. Horowitz, G. Metzger, A new analysis of thermogravimetric traces, Analytical chemistry, 35 (1963) 1464-1468.

[39] A.A. Frost, R.G. Pearson, Kinetics and Mechanism John Wiley and Sons, Inc., New York, (1961) 19.

[40] I. Kenawy, M. Hafez, R. Lashein, Thermal decomposition of chloromethylated poly (styrene)-PAN resin and its complexes with some transition metal ions, Journal of thermal analysis and calorimetry, 65 (2001) 723-736.

[41] P. Maravalli, T. Goudar, Thermal and spectral studies of 3-N-methyl-morpholino-4-amino-5-mercapto-1, 2, 4-triazole and 3-N-methyl-piperidino-4-amino-5-mercapto-1, 2, 4-triazole complexes of cobalt (II), nickel (II) and copper (II), Thermochimica acta, 325 (1999) 35-41.

[42] S.S. Kandil, G.B. El-Hefnawy, E.A. Baker, Thermal and spectral studies of 5-(phenylazo)-2-thiohydantoin and 5-(2-hydroxyphenylazo)-2-thiohydantoin complexes of cobalt (II), nickel (II) and copper (II), Thermochimica acta, 414 (2004) 105-113.

[43] R. Zaky, T. Yousef, Spectral, magnetic, thermal, molecular modelling, ESR studies and antimicrobial activity of (E)-3-(2-(2-hydroxybenzylidene) hydrazinyl)-3-oxo-n (thiazole-2-yl) propanamide complexes, Journal of Molecular Structure, 1002 (2011) 76-85.

[44] R. Zaky, T. Yousef, K. Ibrahim, Co (II), Cd (II), Hg (II) and U (VI) O2 complexes of o-hydroxyacetophenone [N-(3-hydroxy-2-naphthoyl)] hydrazone: physicochemical study, thermal studies and antimicrobial activity, Spectrochimica Acta Part A: Molecular and Biomolecular Spectroscopy, 97 (2012) 683-694.

[45] T. Yousef, Structural, optical, morphology characterization and DFT studies of nano sized Cu (II) complexes containing schiff base using green synthesis, Journal of Molecular Structure, 1215 (2020) 128180.

[46] R.G. Pearson, Absolute electronegativity and hardness: applications to organic chemistry, J. Org. Chem., 54 (1989) 1423-1430.

[47] J. Padmanabhan, R. Parthasarathi, V. Subramanian, P. Chattaraj, Electrophilicity-based charge transfer descriptor, J. Phys. Chem. A, 111 (2007) 1358-1361.

[48] G.A. El-Reash, O. El-Gammal, S. Ghazy, A. Radwan, Characterization and biological studies on Co (II), Ni (II) and Cu (II) complexes of carbohydrazones ending by pyridyl ring, Spectrochimica Acta Part A: Molecular and Biomolecular Spectroscopy, 104 (2013) 26-34.

[49] G.A. El-Reash, O. El-Gammal, A. Radwan, Molecular structure and biological studies on Cr (III), Mn (II) and Fe (III) complexes of heterocyclic carbohydrazone ligand, Spectrochimica Acta Part A: Molecular and Biomolecular Spectroscopy, 121 (2014) 259-267.

[50] S.E.-S. Ghazy, S.E.-S. Samra, A.E.-F.M. Mahdy, S.M. EL-MORSY, Removal of aluminum from some water samples by sorptive-flotation using powdered modified activated carbon as a sorbent and oleic acid as a surfactant, Anal. Sci., 22 (2006) 377-382.

[51] V.I. Klassen, V.A. Mokrousov, An introduction to the theory of flotation, Butterworths, 1963.

[52] S.E.-S. Ghazy, G.A.-H. Moustafa, Flotation-Separation of Chromium (VI) and Chromium (III) from Water and Leathers Tanning Waste Using Active Charcoal and Oleic Acid Surfactant, Bull. Chem. Soc. Jpn., 74 (2001) 1273-1278.

[53] T. Yousef, G.A. El-Reash, O. El-Gammal, S.F. Ahmed, Structural, DFT and biological studies on Cu (II) complexes of semi and thiosemicarbazide ligands derived from diketo hydrazide, Polyhedron, 81 (2014) 749-763.

[54] T. Yousef, G.A. El-Reash, Synthesis, and biological evaluation of complexes based on thiosemicarbazone ligand, Journal of Molecular Structure, 1201 (2020) 127180.

Tables

Table 1. Physical and analytical data of H_4MDI and its metal complexes.

Compound		Color	M.P., (ºC)	% Found (% calcd.)					% Yield
Molecular formula	F.wt			M	Cl	C	H	N	
H_4MDI		Yellow	230	□□□	□□□	58.14	3.14	21.39	95
$C_{19}H_{14}O_4N_6$	390.36					(58.46)	(3.61)	(21.53)	
$[Cr_2(H_2MDI)(H_2O)_2Cl_4]$		Pink	>300	15.41	21.33	34.16	2.66	12.96	78
$C_{19}H_{16}Cl_4Cr_2N_6O_6$	670.18			(15.52)	(21.16)	(34.05)	(2.41)	(12.54)	
$[Ni_2(MDI)(H_2O)_6]4H_2O$		Brown	>300	17.24	□□□	33.78	4.27	12.65	85
$C_{19}H_{30}Ni_2N_6O_{14}$	683.86			(17.16)		(33.37)	(4.42)	(12.29)	

Table 2. Assignments of the IR spectral bands of H_4MDI and its metal complexes.

Compound	(C=O) hydrazide	(C=O) isatin	(C=N) azomethine	(N-H)	(C=N)	(C-O)	(N-N)	(-OH)	(M-O)	(M-N)
H_4MDI	1697	1733	1611	3237	-	1116	1004	3464	-	-
$[Cr_2(H_2MDI)(H_2O)_2Cl_4]$	-	1703	1617	3218	1617	1198	1013	3418	520	488
$[Ni_2(MDI)(H_2O)_6]4H_2O$	-	-	1655	-	1621	1206	1016	-	550	499

Table 3. Electronic spectral data and magnetic moment of H_4MDI and its metal complexes.

Compound	Band position, cm^{-1}	μ_{eff} (BM)
H_4MDI	32258, 27932, 22935	-
$[Cr_2(H_2MDI)(H_2O)_2Cl_4]$	32051, 27932, 22831	3.51
$[Ni_2(MDI)(H_2O)_6]4H_2O$	32051, 27777, 21551, 20552, 19157	2.76

Table 4. Thermal behavior for metal complexes of H_4MDI.

Complex	Temp. range,°C	Removed species	Wt. loss	
			Found%	Calcd.%
$[Cr_2(H_2MDI)(H_2O)_2Cl_4]$	220.53-325.54	$2H_2O$	-	-
$[Ni_2(MDI)(H_2O)_6].4H_2O$	33.09-90.88	$4H_2O$	10.60	10.54
	154.10-244.58	$6H_2O$	-	-

Table 5. Kinetic parameters evaluated by Horowitz-Metzger (HM) and Coats-Redfern (CR) equations for complexes of H_4MDI.

Compound	Step	Mid temp., K	Model	E_a	A	ΔH*	ΔS*	ΔG*
				KJ/mol	(S^{-1})	KJ/mol	KJ/mol.K	KJ/mol
$[Cr_2(H_2MDI)(H_2O)_2Cl_4]$	1st	557.35	HM	143.82	1.12×10^{11}	139.19	-0.0386	160.68
			CR	137.07	2.78×10^{10}	132.44	-0.0502	160.41
	2nd	660.05	HM	271.06	9.09×10^{18}	265.57	0.1114	192.03
			CR	269.88	7.66×10^{18}	264.39	0.1100	191.78
	3rd	817.45	HM	258.66	7.15×10^{13}	251.87	0.0119	242.11
			CR	254.77	4.23×10^{13}	247.97	0.0076	241.78
	4th	938.34	HM	544.08	6.37×10^{27}	536.28	0.2778	275.58
			CR	543.13	5.79×10^{27}	535.33	0.2770	275.37
	5th	1035.41	HM	826.59	1.32×10^{39}	817.98	0.4937	306.84
			CR	826.83	1.39×10^{39}	818.22	0.4941	306.65
$[Ni_2(MDI)(H_2O)_6].4H_2O$	1st	337.13	HM	64.42	7.98×10^{7}	61.62	-0.0947	93.53
			CR	59.01	1.22×10^{7}	56.20	-0.1103	93.38
	2nd	503.81	HM	395.92	1.63×10^{39}	391.73	0.5014	139.12
			CR	390.94	5.07×10^{38}	386.75	0.4917	139.03
	3rd	564.76	HM	234.46	6.32×10^{19}	229.77	0.1288	157.00
			CR	223.40	6.06×10^{18}	218.70	0.1094	156.94
	4th	785.92	HM	517.00	1.53×10^{32}	510.47	0.3632	225.04
			CR	508.23	4.10×10^{31}	501.69	0.3522	224.87

Table 6. Calculated E_{HOMO}, E_{LUMO}, energy band gap ($E_H - E_L$), electronegativity (χ), chemical potential (μ), global hardness (η), global softness (S) and global electrophilicity index (ω), and softness (𝛘) for H_4MDI and thier complexes.

Compound	E_H (eV)	E_L (eV)	$(E_H - E_L)$ (eV)	χ (eV)	μ (eV)	η (eV)	S (eV^{-1})	ω (eV)	⍰ (eV)
H_4MDI	-5.239	-3.319	-1.920	4.279	-4.279	0.960	0.480	9.536	1.042
$[Cr_2(H_2MDI)(H_2O)_2Cl_4]$	-3.913	-3.572	-0.341	3.743	-3.743	0.171	0.085	41.074	5.865
$[Ni_2(MDI)(H_2O)_6].4H_2O$	-3.454	-3.066	-0.388	3.260	-3.260	0.194	0.097	27.391	5.155

Table 7. Removal % of 4×10^{-4} of Ni(II) in the presence of some selected foreign ions [4×10^{-4} mol/L of H_4MDI, 1×10^{-3} mol/L of HOL at pH 7].

Interfering ions		Added salt	Tolerable limit (μg/mL)	Re %
Anions	Cl^-	NaCl	1000	98.4
	SO_4^{2-}	Na_2SO_4	800	94.9
	HCO_3^-	$NaHCO_3$	1000	99.5
	CH_3COO^-	CH_3COONa	180	99.2
	NO_3^-	$NaNO_3$	900	97.3
Cations	NH_4^+	NH_4Cl	250	97.8
	Na^+	NaCl	1000	99.3
	K^+	KCl	1000	98.4
	Mg^{2+}	$MgCl_2$	100	100
	Ca^{2+}	$CaCl_2$	100	97.5
	Ba^{2+}	$BaCl_2$	120	96.1

Table 8. Removal % of Ni(II) added to some real water samples [4×10^{-4} mol/L of H_4MDI, 1×10^{-3} mol/L HOL at pH 7].

Table 9. Antibacterial and antifungal activities of H_4MDI and its metal complexes in terms of MIC (μg/mL).

Sample		Bacteria		Fungi
		E. coli	*S. aureus*	*C. Albicans*
Standard	Ciprofloxacin	1.56	0.78	----
	Fluconazole	----	----	1.17
H_4MDI		0.78	3.12	0.78
Cr(III)-H_4MDI		37.5	12.5	4.68
Ni(II)-H_4MDI		4.68	2.34	1.17

Sample type	Sample location	Re %
Distilled water	Our laboratory	100.0
Tap water	Mansoura	97.2
Nile water	Mansoura	99.3
	Kafr El-Sheikh	93.8
Drinking water	Mansoura	97.5
	Cairo	99.0
	Tanta	97.5
Underground water	Mansoura	95.0

Table 10. ***In-vitro*** **cytotoxic activity of ligand (H_4MDI) and its metal complexes against human tumor cells hepatocellular carcinoma (HePG-2).**

Compound	*In-vitro* Cytotoxicity IC_{50} (µmol/L)
5-fluorouracil	7.9±0.84
H_4MDI	9.7±1.04
Cr(III)-H_4MDI	20.3±1.35
Ni(II)-H_4MDI	7.7±0.72

Figures

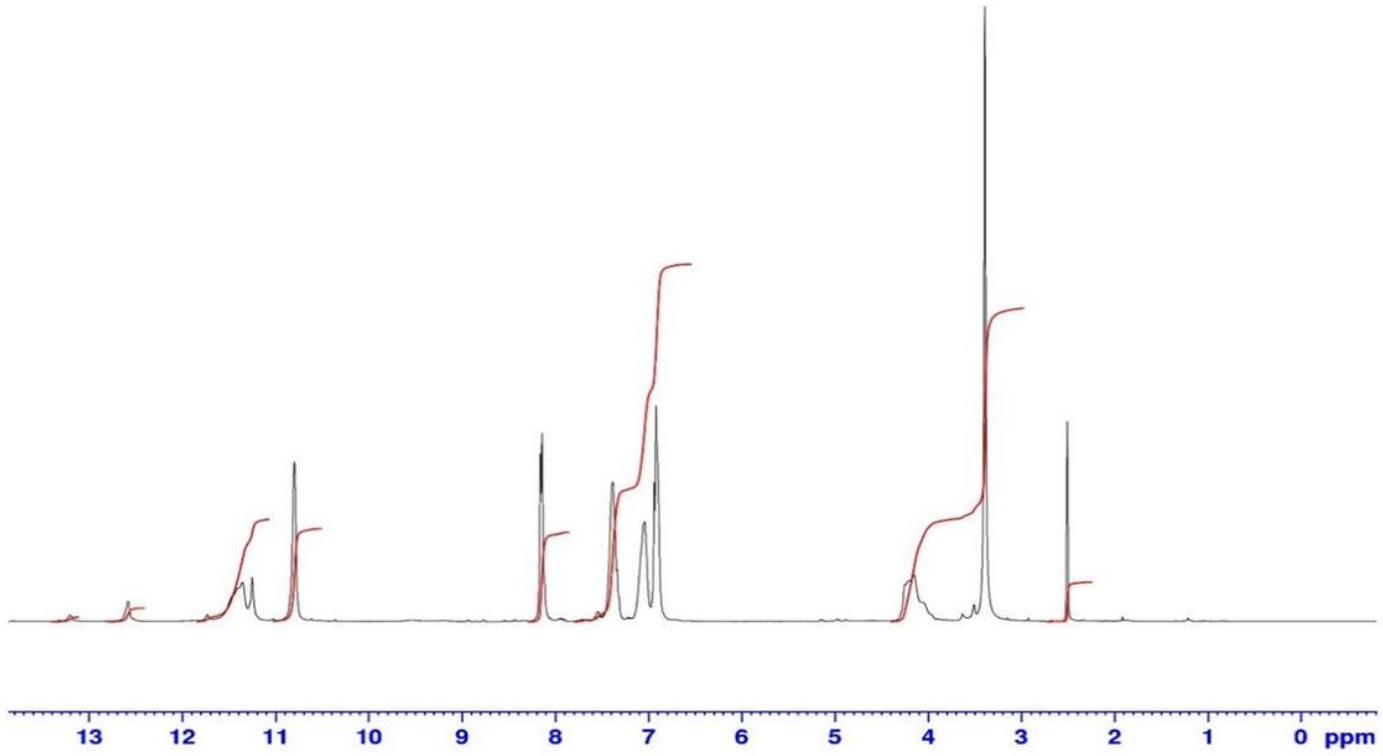

Figure 1

1H-NMR spectra of H4MDI.

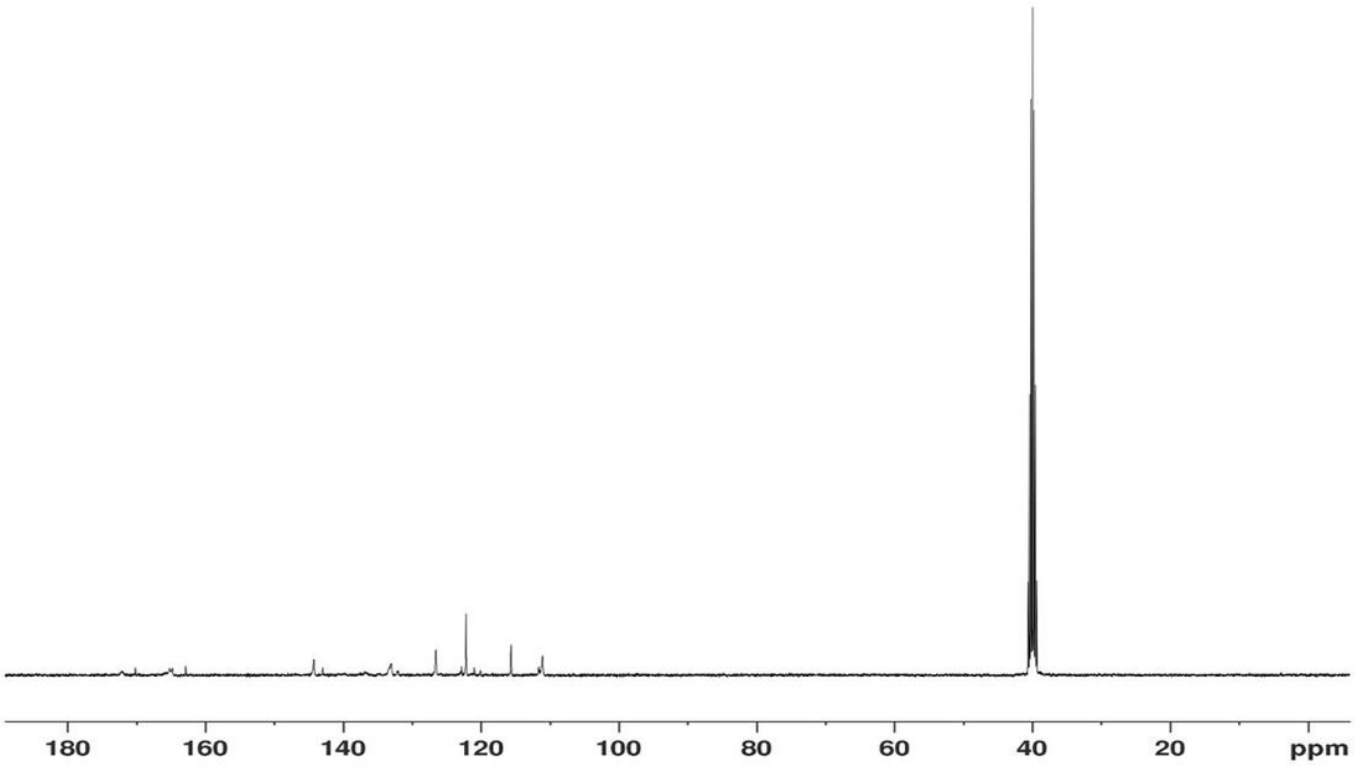

Figure 2

13C-NMR spectra of H4MDI.

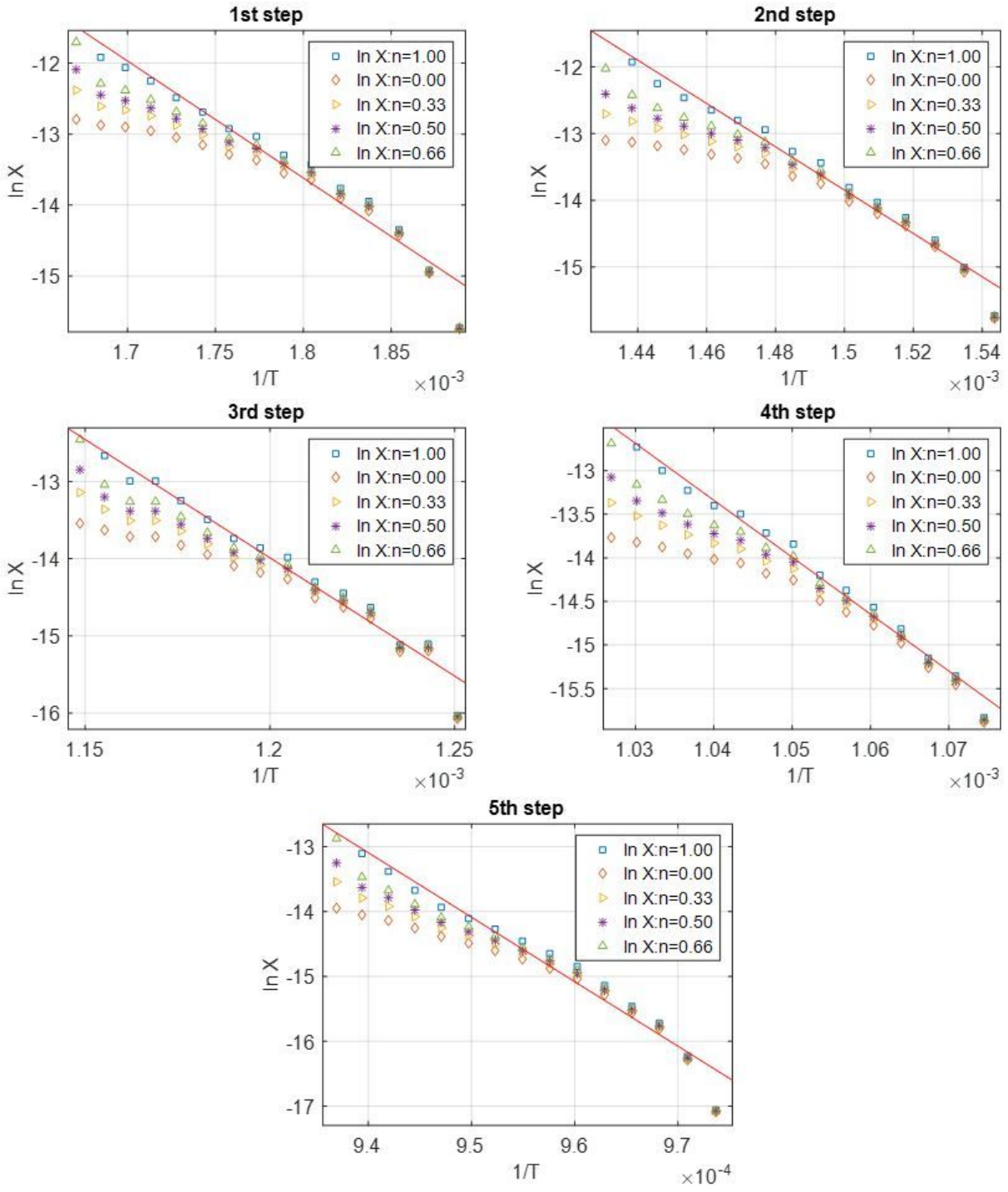

Figure 3

Coats-Redfern plots of [Cr2(H2MDI)(H2O)2Cl4].

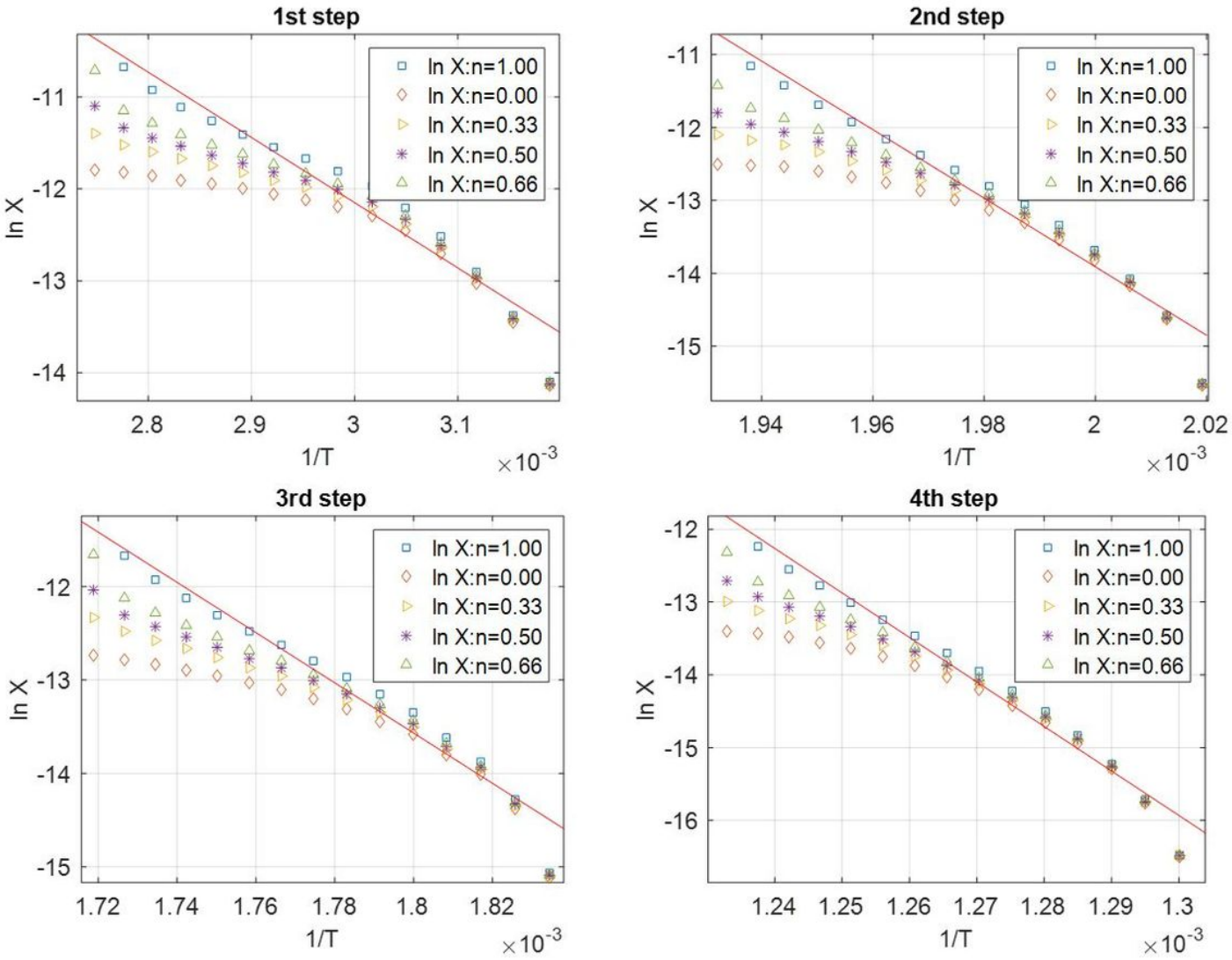

Figure 4

Coats-Redfern plots of [Ni2(MDI)(H2O)6].4H2O.

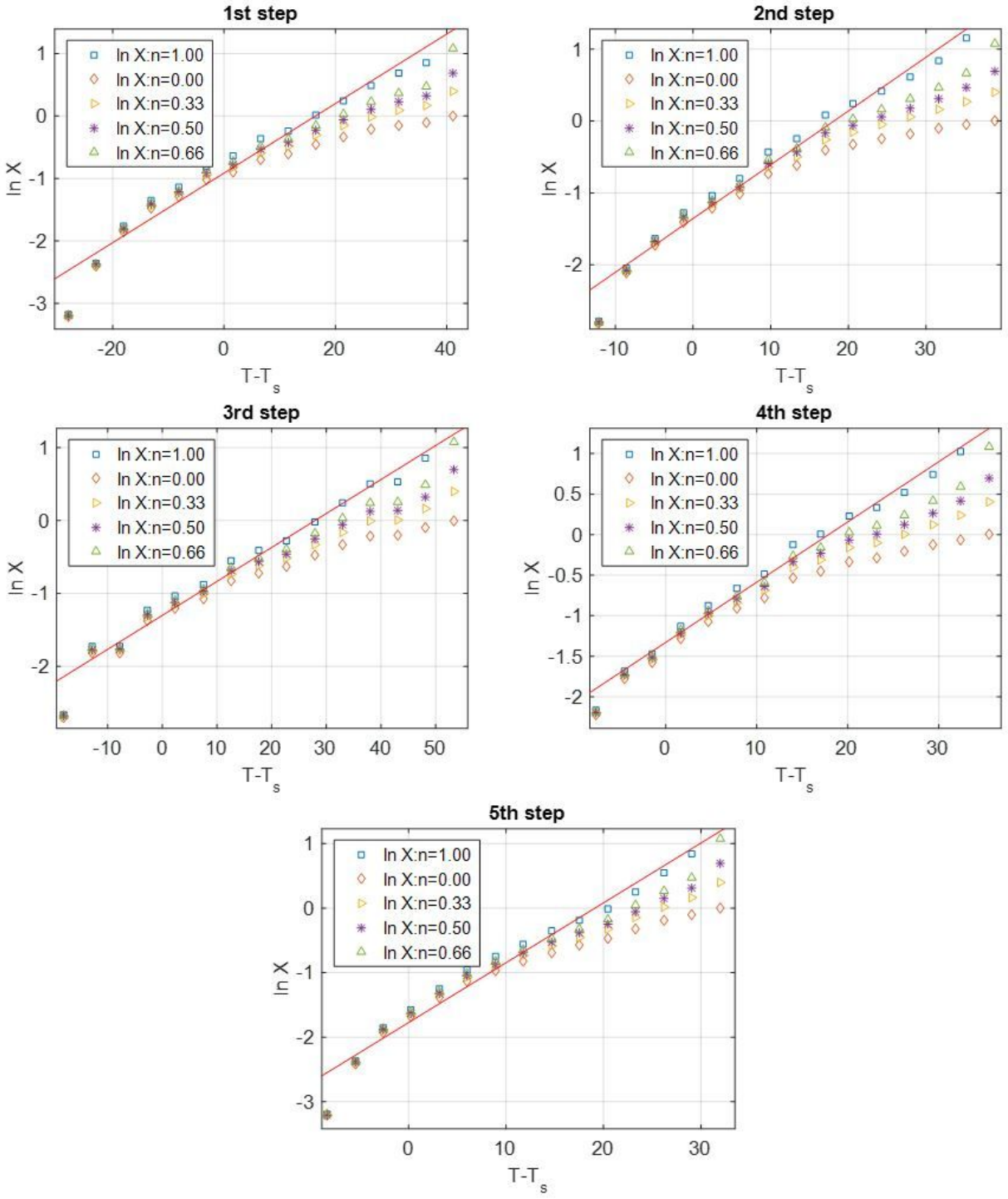

Figure 5

Horowitz-Metzger plots of [Cr2(H2MDI)(H2O)2Cl4].

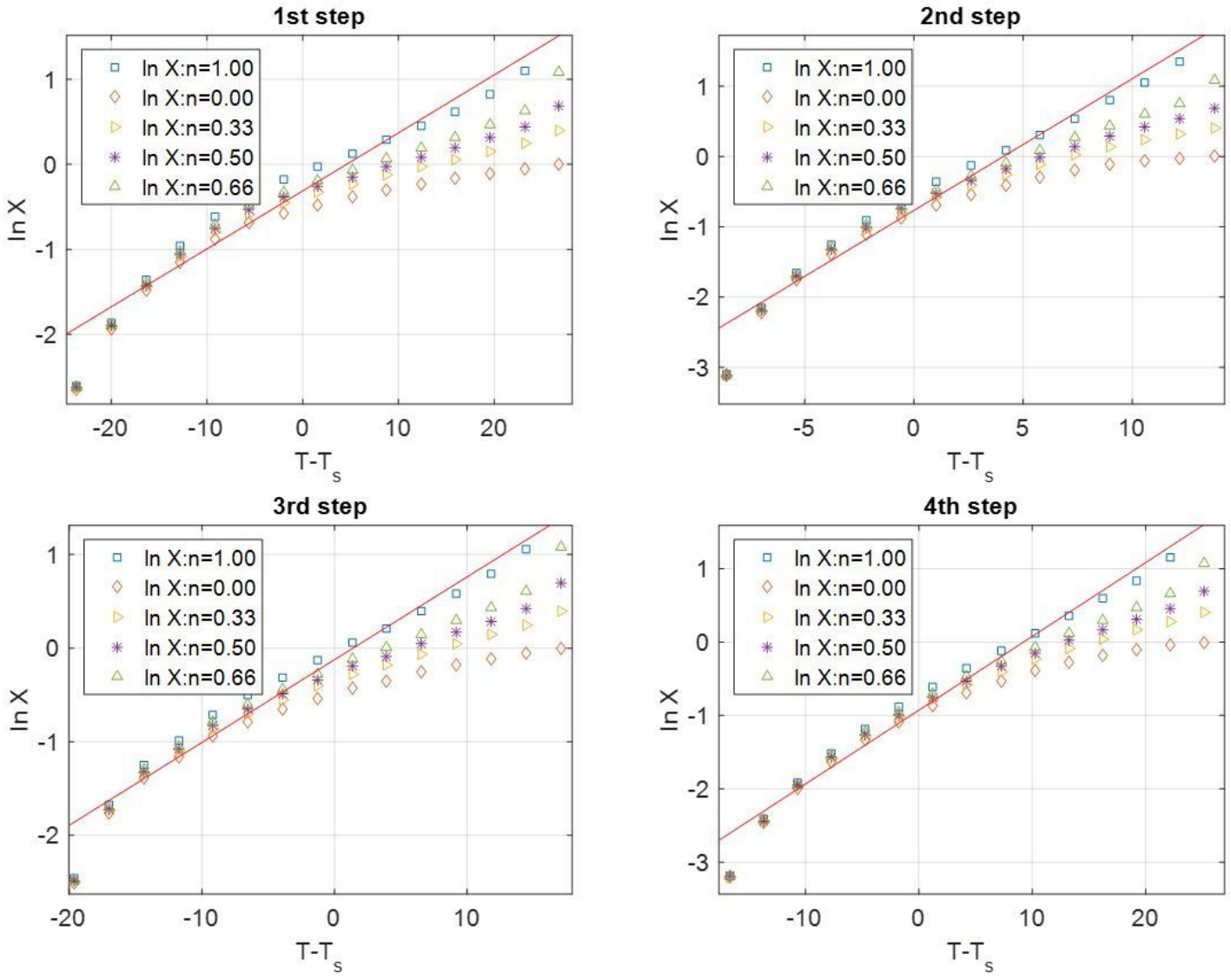

Figure 6

Horowitz-Metzger plots of [Ni2(MDI)(H2O)6].4H2O.

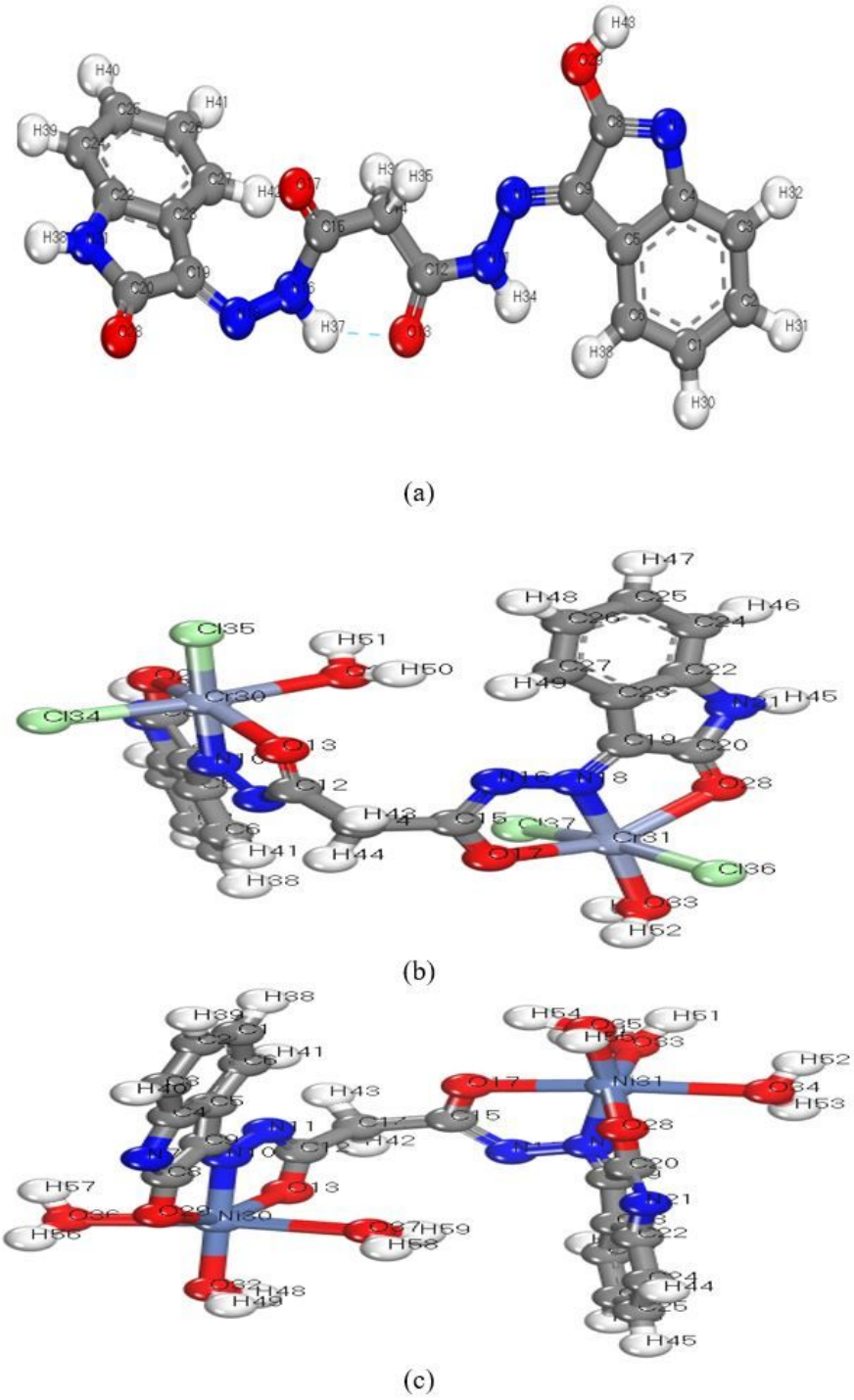

Figure 7

Molecular modelling along with the atom numbering scheme of (a) H4MDI, (b) [Cr2(H2MDI)(H2O)2Cl4], and (c) [Ni2(MDI)(H2O)6].4H2O.

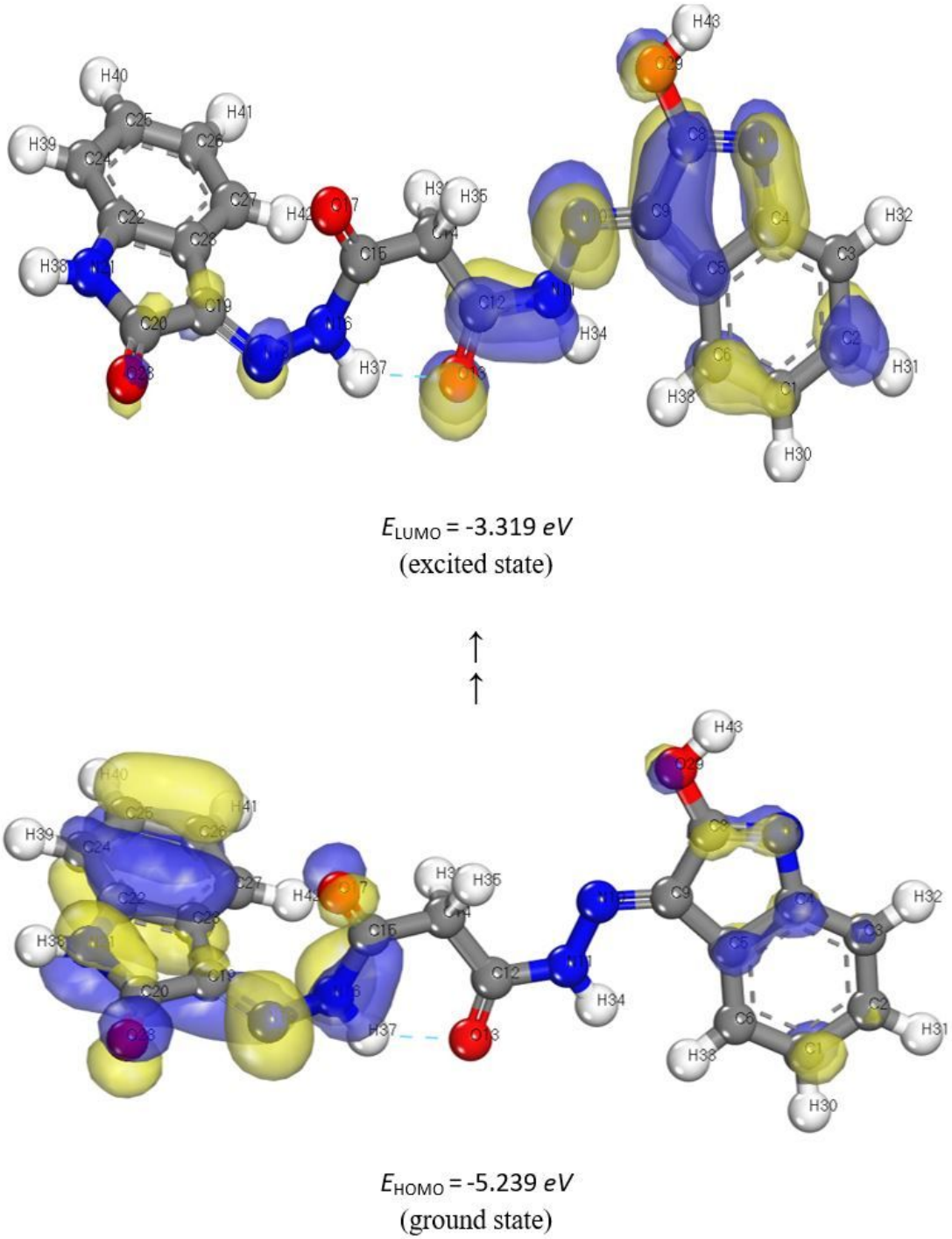

Figure 8

3D-plots of frontier orbital energies using DFT method for H4MDI.

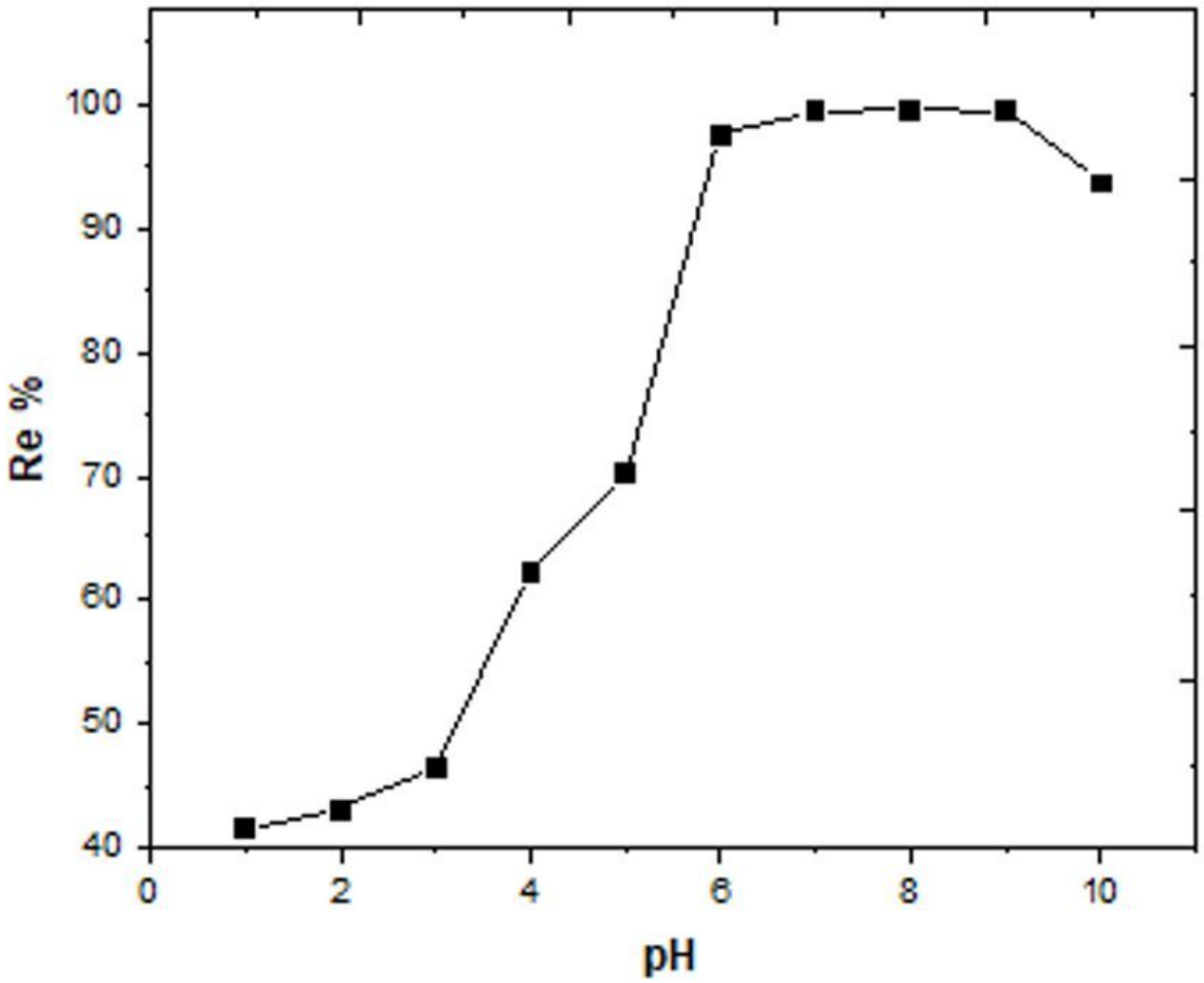

Figure 9

Effect of pH on the removal % of 4×10-4 mol/L of Ni(II) using 4×10-4 mol/L of prepared ligand and 1×10-3 mol/L of HOL.

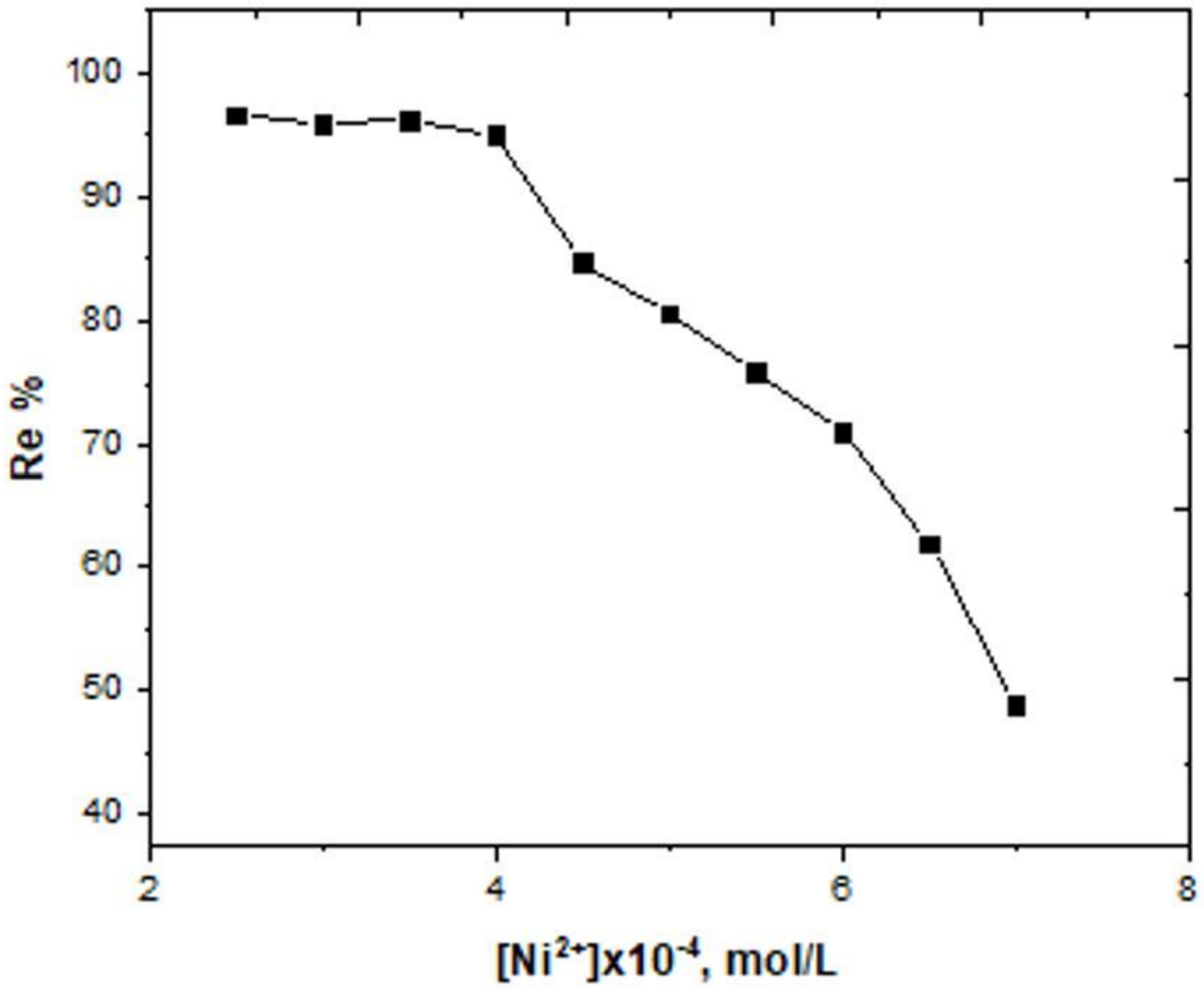

Figure 10

Removal % of different concentrations of Ni(II) using 4×10-4 mol/L of prepared ligand and 1×10-3 mol/L of HOL at pH 7.

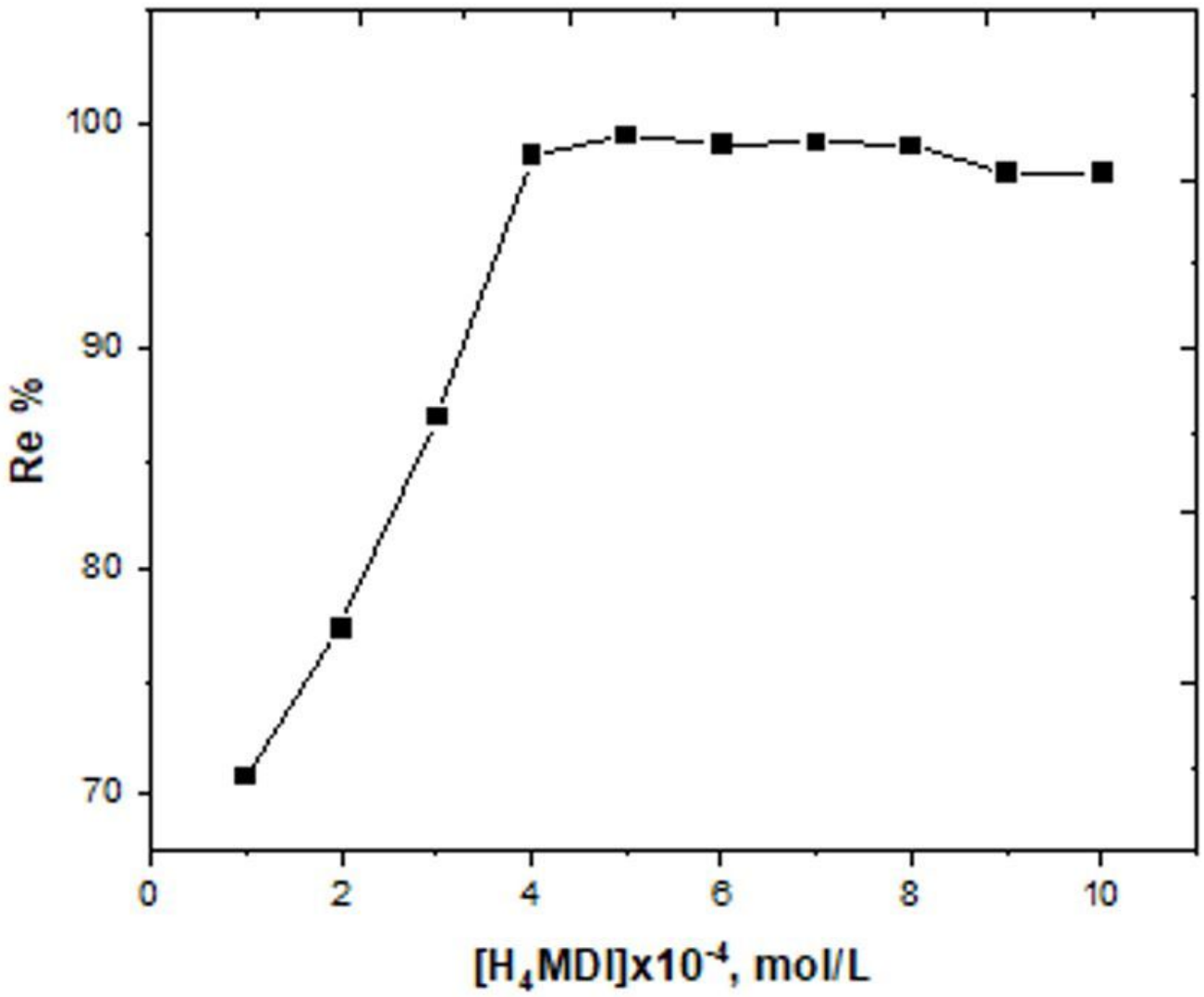

Figure 11

Removal % of 4×10-4 mol/L of Ni(II) using different concentrations of prepared ligand and 1×10-3 mol/L of HOL at pH 7.

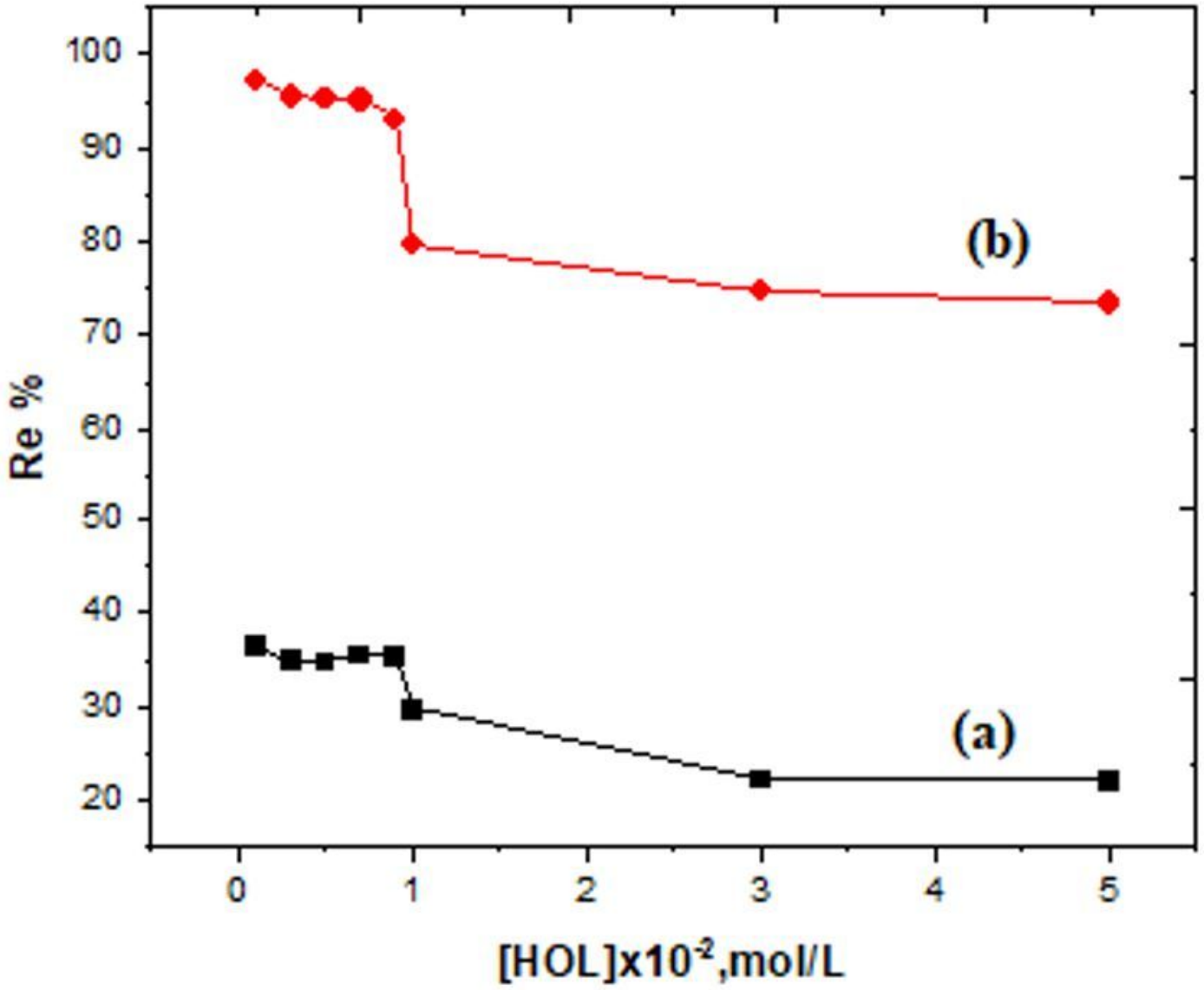

Figure 12

Removal % of 4×10-4 mol/L of Ni(II) using different concentrations of HOL in the absence (a) and presence (b) of 4×10-4 mol/L of prepared ligand at pH 7.

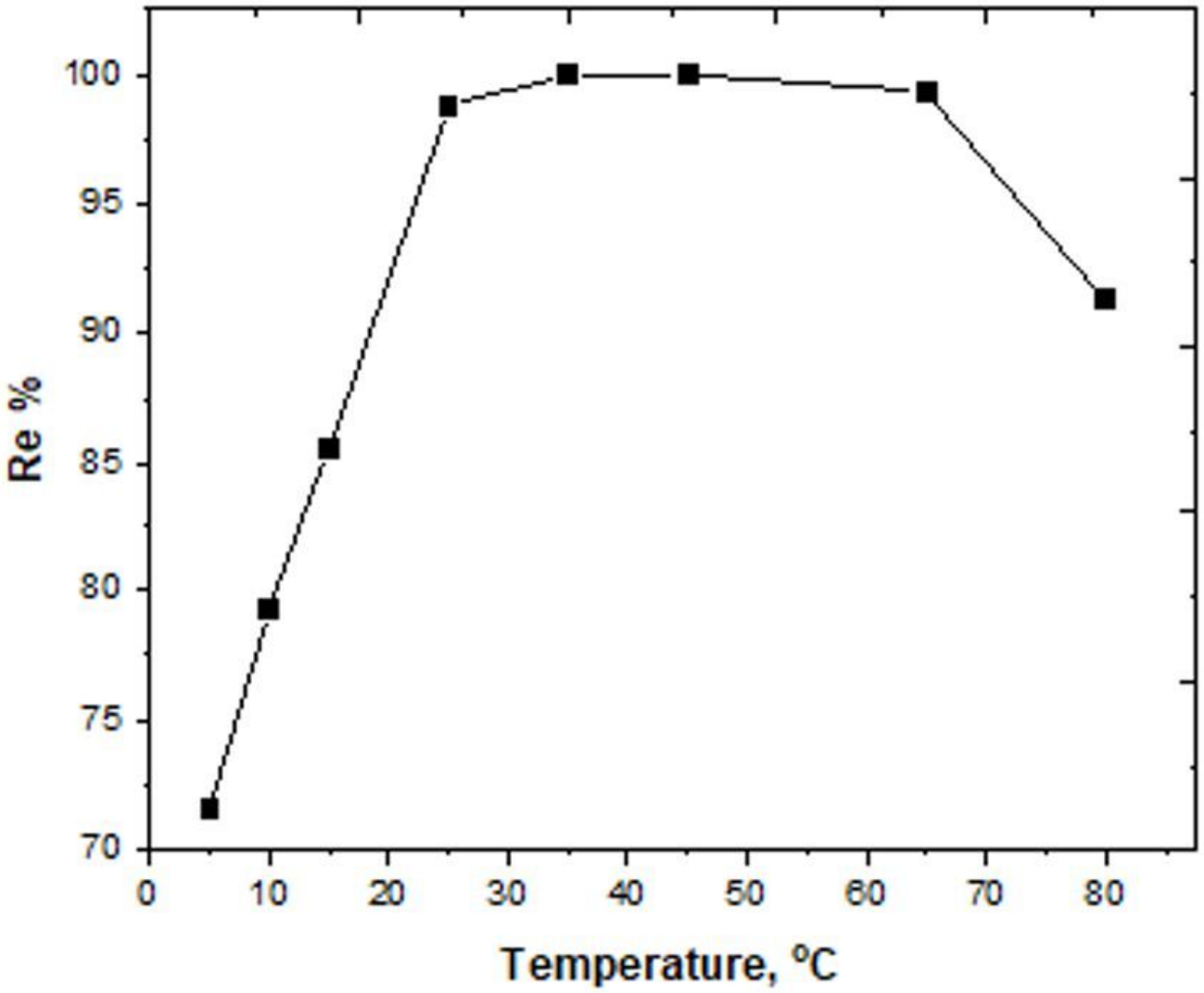

Figure 13

Removal % of 4×10-4 mol/L of Ni(II) at different temperatures using 4×10-4 mol/L of prepared ligand and 1×10-3 mol/L HOL at pH 7.

Supplementary Files

This is a list of supplementary files associated with this preprint. Click to download.

- scheme1.jpg
- Supplementarymaterial.docx